Int. J. Heat Mass Transfer. Vol. 36, No. 6, pp. 1553–1571, 1993
Printed in Great Britain

0017-9310/93 $6.00 + 0.00

Transient forced convection heat transfer in a vertical rib-heated channel using a turbulence promoter

H. H. LIN and Y. H. HUNG
Department of Power Mechanical Engineering, National Tsing Hua University, Hsinchu, Taiwan 30043, R.O.C.

(*Received* 28 *January* 1992 *and in final form* 1 *July* 1992)

Abstract—An experimental investigation for transient forced convection heat transfer in a vertical rib-heated channel with a turbulence promoter has been systematically performed. Parametric studies including the steady-state convective heat flux, channel inlet velocity, channel spacing, and promoter location and height on transient heat transfer performance in a vertical rib-heated channel have been explored. A generalized distribution for transient convective heat flux is proposed; the channel inlet velocity is verified to be the most significant parameter affecting transient convective heat flux and Nusselt number distributions. Besides, the use of a turbulence promoter can effectively enhance transient heat transfer performances for all the ribs in both the entrance and the fully-developed regions of the channel. Furthermore, the present results reveal that the effect of channel inlet velocity is more significant on the heat transfer performance of ribs in the entrance region than in the fully-developed region of the channel, while the effect of promoter height is reverse. The effect of promoter height compared with that of promoter location has more significance on heat transfer performance in the fully-developed region.

INTRODUCTION

HEAT TRANSFER from discrete heat sources deployed along one wall of a vertical channel, which is used to simulate the printed circuit boards (PCBs) in modern electronics packaging, has received increasing attention in the last decade because of the close packing of electronic components and the high heat dissipation rates in modern PCBs. Typically, the thermal design of PCBs requires that the junction temperatures of electronic components mounted on the boards be maintained below 125°C, while the component case temperature is between 85 and 100°C by reliability considerations. If the thermal control is incorrect, the excessive temperature will cause the electronic components and equipment to malfunction or burn out. Moreover, investigations have demonstrated that a single electronic component operating 10°C beyond the maximum temperature can readily reduce the reliability of some systems by as much as 50% [1]. Therefore, how to cool the electronic components effectively and keep them reliable becomes a very important issue for the thermal design of electronics packaging. Consequently, the selection of effective cooling systems is an essential task for the above purpose. For moderate heat dissipation rates, forced air cooling with a variety of heat transfer enhancement techniques has been found to be a preferable cost effective option in addition to its inherent reliability and mechanical simplicity. Therefore, the research of heat transfer and fluid flow in the field of forced convection air cooling is demanded for the need of assuring the reliability of PCBs.

Most recent studies concentrated on the steady-state heat transfer characteristics in the periodically fully-developed (or the so-called 'quasi-equilibrium' high temperature) region for forced air cooling of a vertical channel with two-dimensional discrete rectangular heating ribs or three-dimensional heating blocks. Not much work has been done to explore local heat transfer characteristics in the entrance region of the channel. Conceptually, the entrance heat transfer coefficient being high, an accurate estimation of its value is of importance for thermal design. The components with higher heat dissipation rates can then be placed in the entrance region to achieve more efficient cooling of PCBs.

In 1981, Arvizu and Moffat [2] presented heat transfer results for a dense array of flat packs. They found that the heat transfer coefficients were greatest on the first row and then dropped to a fully-developed value by the third row of the flat packs. The periodically fully-developed heat transfer results for the ribbed geometry were verified to have the relationship of $Nu = C\,Re^{0.75}$ except for very close spacings, e.g. $S/B \leqslant 2.5$, where the high rib density begins to take on nearly parallel plane flow and $Nu \propto Re^{0.8}$. In 1982, Sparrow *et al.* [3] used the naphthalene sublimation technique to measure the Sherwood number and inferred a Nusselt number for modules, and then explored the heat transfer and pressure drop for forced convection in arrays of heat generating rectangular modules deployed along one wall of a horizontal flat rectangular duct, with and without barriers, and missing modules. Air was the mass transfer medium in the experiments. For a fully populated

NOMENCLATURE

B rib height
C_p specific heat at constant pressure
H channel spacing
h heat transfer coefficient based on inlet temperature, $q_c''/(T_w - T_0)$
k thermal conductivity
L rib length
L_t total heating length of each rib, $2B+L$
LP location of turbulence promoter ($LP = 1, 2, 3$, or 4), shown in Fig. 1
Nu Nusselt number based on inlet temperature, $q_c''B/k(T_w - T_0)$
Q heat flow rate
q'' heat flux
R electrical resistance
Re channel Reynolds number, $\rho U_0 H/\mu$
r_{fd} heat transfer defect from the first rib of entrance region to the rib of the fully-developed region, Nu_{fd}/Nu_1
S streamwise pitch of two adjacent ribs
T temperature
t time or turbulence promoter height
U velocity
V voltage or volume.

Greek symbols
μ dynamic viscosity
ρ density.

Superscript
$\bar{}$ average.

Subscripts
b balsa wood
c convection
fd fully-developed region
i total
j rib number
k conduction
0 at channel inlet
r radiation
s steady-state or stainless steel sheet
t transient
w rib surface
x local.

array without barriers, periodically fully-developed heat transfer coefficients were encountered for the fifth and all subsequent rows. The implantation of a barrier in the module array was shown to be an effective enhancement device, with the greatest effect being felt in the second row downstream of the barrier, while residual enhancement persisted considerably further downstream in their study. However, at the module immediately upstream of the barrier, there was a reduction in the heat transfer coefficient. In 1983 and 1984, Sparrow *et al.* explored the same problem by using multiple fence-like barriers, with the interbarrier spacing and the barrier height varied parametrically along with the Reynolds number [4, 5]. The main objective in ref. [4] was to determine the individual heat transfer coefficients at the top and side surfaces of the modules. Perspectives on heat transfer and pressure drop results were provided by flow visualizations performed using the oil–lampblack technique. Furthermore, the convective heat transfer response to height differences in an array of block-like electronic components was again investigated experimentally by Sparrow *et al.* [5].

More recently, laminar flow and conjugate heat transfer across three identical two-dimensional rectangular protruding blocks were theoretically analyzed using a finite difference method by Davalath and Bayazitoglu [6]. Local and average component Nusselt numbers were presented for several channel Reynolds and fluid Prandtl numbers. Furthermore, three-dimensional numerical solutions without turbulence promoters were provided by Asako and Faghri [7, 8]. Results were obtained for periodically fully-developed laminar flow and heat transfer over three-dimensional rectangular protrusions with the condition of uniform wall temperature. Supplementary computation showed that the friction factor and the Nusselt number could be predicted by two-dimensional models, depending on the geometric parameters. As with the predictions in ref. [6], the highest local Nusselt numbers along the protrusion were found near the leading edge of the face oriented parallel to the flow direction. As for the periodically fully-developed turbulent flow and heat transfer in two-dimensional ducts with rectangular protrusions, Knight and Crawford employed the k–ε turbulence model to account for turbulence transport in the system [9, 10]. Their predictions showed good agreement with the experimental results presented by Lehmann and Wirtz [11].

In 1988, Tarikoshi *et al.* [12] also presented entrance heat transfer coefficient results for uniform block heights as well as arrays consisting of blocks of different heights. For uniform block height, the heat transfer coefficient trend is consistent with the literature for flat packs and falls off to the periodically fully-developed value, i.e. the maximum at the first row. For abrupt changes of block height, however, no distinct trend was observable.

In 1990, McEntire and Webb [13] conducted a series of experiments to measure the local forced convective heat transfer characteristics of an array of protruding

and flush-mounted two-dimensional discrete heat sources in a vertical channel. Air flow rates yielding effective channel Reynolds numbers Re in the range of 525–3937 were employed. The results of their experiments showed that the protruding heat sources yielded higher heat transfer than flush-mounted heat sources at the same channel Reynolds number. The interruption of the thermal boundary layer in the adiabatic sections between the heaters results in heat transfer enhancement. Chao [14] experimentally dealt with transient and steady-state forced convection heat transfer in a vertical rib-heated channel without a turbulence promoter. In his study, when the channel inlet velocity was higher than 1.27 m s^{-1}, a generalized correlation for transient convective heat flux was proposed, while it would reasonably tend toward the natural convection correlation proposed by Chang [15] when the channel inlet velocity is gradually decreased from 1.27 m s^{-1}. In addition, the effects of parameters such as channel spacing, steady-state convective heat flux, and channel inlet velocity on heat transfer performance of heating ribs were investigated extensively. It was also found that the periodically fully-developed region starts at the third rib in the range of channel Reynolds number $Re = 2182$–29 696. In 1991, Faghri *et al.* [16] reported the local heat transfer data in the channel entrance region of regular in-line arrays of rectangular blocks in forced air cooling. The study of Nusselt number profile in their paper showed that the module-averaged Nusselt numbers in the entrance region are usually high and fall off to periodic fully-developed values by the third or fourth row of the array. Also, the entrance Nusselt number is a strong function of channel inlet velocity.

As we know, the use of barriers or turbulence promoters in rib-heated channels has been corroborated to be a simple but effective means for enhancing heat transfer performance. Although turbulence promoters lead to a locally high pressure drop, they can generate a locally suddenly accelerated flow with a high level of turbulence and thus result in a local heat transfer enhancement in the channel. In 1991, a new installation of turbulence promoter, which was proposed to be mounted on the opposite shrouding insulated wall in the rib-heated channel by Hung and Lin [17], was shown to be better than those studied in refs. [3, 4]. The installation could effectively enhance all the rib heat transfer performances in the channel and avoid hot spots occurring in the fully-developed (or 'quasi-equilibrium') high temperature region. From their results, it was found that the fully-developed region started at the third rib. This was consistent with the same trend observed in refs. [2, 14, 16]. Furthermore, the greatest Nusselt number enhancement occurred at the rib immediately downstream of the promoter. With increasing upstream or downstream distance of the heating rib from the promoter, the extent of the heat transfer enhancement gradually dropped off. In addition, the steady-state rib heat transfer performance increased with decreasing H/B ratio. The effect of steady-state convective heat flux on steady-state rib heat transfer performance was insignificant; while the effect of channel inlet velocity was significant, the rib steady-state heat transfer performance increased with increasing channel inlet velocity. The t/H effect was, compared with the effect of promoter location, more significant on steady-state heat transfer performance. The steady-state Nusselt number increased with increasing t/H ratio.

The foregoing literature survey indicates that most existing work has dealt only with steady-state heat transfer from discrete heated sources in a channel, for the most part in the periodically fully-developed region. Moreover, although the barrier implanted on the module-sublimated wall has been studied in refs. [3–5], little information on the effect of a turbulence promoter, implanted on the opposite shrouding insulated wall, on the transient local thermal characteristics in a rib-heated channel is available in the existing literature. In order to advance our understanding of transient heat transfer performance in a vertical rib-heated channel with a turbulence promoter, a series of systematic experiments have been conducted in this paper. Studies of parameters influencing the transient thermal characteristics of forced convection in a vertical rib-heated channel using turbulence promoters are performed. This work is an extension of earlier steady-state experimental investigations on the same channel [17]. Thus, the objective of this research is to experimentally explore the effects of relevant influencing parameters such as the channel spacing, steady-state convective heat flux, channel inlet velocity, and promoter location and height on transient forced convection heat transfer characteristics in a vertical rib-heated channel utilizing turbulence promoters.

EXPERIMENTAL SET-UP AND PROCEDURES

The present transient experiments were performed in a low-turbulence open-loop wind tunnel, which was in a buoyancy-assisting flow condition. The relevant experimental set-up and procedures are briefly described in the following.

Heat transfer experimental facilities

The heat transfer experimental facilities, consisting of the wind tunnel facility, and apparatus and instrumentation used in the present experiments are the same as those employed by Hung and Lin [17]. A detailed description of the general configurations and functions of the facilities can be found in ref. [18].

Rib-heated test channel

The schematic of the test channel used in the experiments with all relevant definitions is shown in Fig. 1. The test channel was composed of two plates: a rib-heated test plate and a shrouding insulated plate.

The rib-heated test plate was 38.0 cm wide, 28.0 cm high, and 0.4 cm thick. There were four rectangular

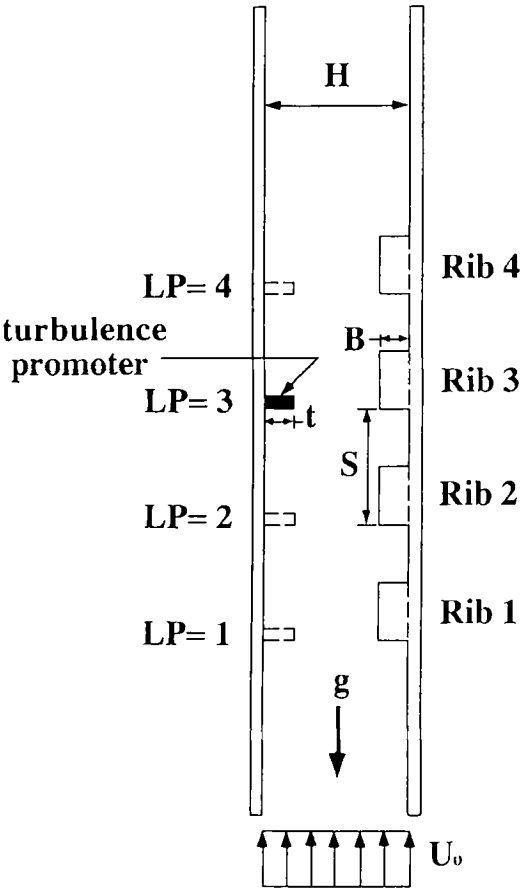

FIG. 1. Test channel investigated in experiments.

heating ribs, which were made of 0.1-cm-thick stainless steel sheets and 0.03-cm-thick thermofoil heaters, with dimensions of $38.0 \times 2.0 \times 1.0$ cm, mounted on the PCB surface. Detailed geometry and composition of the rib-heated test plate has been described and illustrated in ref. [17]. Additionally, a turbulence promoter was mounted on the opposite shrouding insulated wall parallel to the rib-heated test plate. The dimensions of turbulence promoters, which were made of fiberglass material, were 38.0 cm length and 0.4 cm thickness with various heights (i.e. t = 1.0–4.5 cm). A piece of L-shaped metal was attached to each lateral end of the promoter, and two metal bars with 25 screw holes were bolted to the backside of the insulated wall. Thus, the promoter can be slid along the insulated wall to the desired position, and then fastened on the insulated wall with four 1/16 in. screws. Accordingly, the effect of the promoter on flow and thermal characteristics in the vertical rib-heated channel can easily be investigated in the experiments.

Apparatus and instrumentation

The channel spacing between the rib-heated test plate and the shrouding insulated plate was measured by an 150 ± 0.05 mm MITUTOYO vernier caliper. Both the horizontal and vertical of the test plates were calibrated by a water level.

The rib-heated test plate had four 90–110 Ω resistive thermofoil heaters embedded in the rectangular ribs for heating, and 154 calibrated T-type thermocouples epoxied on the specified locations for temperature measurements. Also, the air temperatures at the inlet and outlet of the test channel were also measured with two calibrated T-type thermocouples. Hence, the local transient temperature distributions along the test surface, including the array of ribs as well as the channel inlet/outlet temperatures, could be accurately measured with a FLUKE-2280B data logging system interfaced to PC-At based peripherals. The interface between the computer and the test plate was a 2280 Digital Acquisition and Control Unit. The unit has 160 channels of scannable thermally-compensated relays which are connected to the thermocouples.

Four d.c. power supplies (Model: GW GPD-6030D, maximum ratings: 60 V and 30 A) provided the power to heaters for making the input power changeable. A digital multimeter (Model: YOKOGAWA 2502A; resolution: 1 μV on 100 mV range and 1 mΩ on 100 Ω range) was utilized to calibrate the voltage of each d.c. power supply. In addition, an A-20P-E SEPLC programmable power-source controller was used to control the 'on–off' switches of the blower and power supplies for transient measurement purpose.

As for the velocity measuring system, it included a precise hot wire anemometer (Model: IET V-01-AND) and a Dwyer microtector with high precision on pressure measurements. The microtector delivers repeatable accuracy in measuring positive, negative, or differential pressure to $\pm 0.00025''$ water column over a 0.0–2.0″ W.C. range. Precise calibration between the dynamic pressure head and air velocity, measured by the microtector and by the hot wire anemometer respectively, was made in the experiments.

Static pressure measurements along the opposite shrouding insulated wall were achieved using a series of micro-pressure differential transducers (Model: PR-272) connected to an IBM PC-AT computer with a data acquisition interface card (Model: LABTECH DAS-16) and control software.

To facilitate the interpretation of heat transfer characteristics from four heated ribs in a vertical channel without or with a turbulence promoter placed on the opposite shrouding insulated plate of the channel, flow visualization with the image processing technique was performed in the present study.

Flow visualization instruments consisted of smoke generator, recorder, and illumination accessories. An NPL-type FVSP 204 smoke generator system was selected to produce smoke by vaporizing the hydrocarbon oil (Shell 'Ondina EL' oil) and then the smoke vapor was introduced into the upstream of the test section for flow visualization. The flow-field visualiz-

ation was recorded in order to be digitized by the image processor. Because the flow pattern of the flow-field in the forced convection experiments was continuous, a precision CCD (Charge-Coupled Device) video camera (SONY CCD-V900 Video 8 mm Handycam) was utilized to record flow patterns in the present experiments. This CCD camera has a focus from 11 to 88 mm and a $\times 8$ power zoom factor; thus the smallest smoke structure of the flow pattern could be observed in detail by using the maximum zoom factor. For the sake of observing the recorded flow-field in real time, the CCD camera was connected to an image-processing display system. In addition, in order to record simultaneously the image taken by the CCD camera with a video recorder, the CCD camera was connected to a Hi-Fi Head stereo video recorder (Model: CHUN VR-55HF). Usually, a stable image could be paused and displayed on the monitor by using the 4 Head recorder; thus the image of the flow-field could be grabbed in a more stable and clear mode. The illuminating equipment used in the present research was a PoleStar photo lamp with a 110 V and 300 W input. The lamp was properly placed in the left side of the test-section; the light of the lamp could then pass through the transparent acrylic–plastic material and the opposite shrouding insulated plate to illuminate the smoke for recording flow-fields.

The image-processing devices employed in the experiments were composed of two parts. The first part is the image processor which is used to deal with the image. The second part is the image display which is used to show the image on a monitor. The image processor (Model: FG-1024-3-U-AT-A) developed by Werner Frei Associates with two relevant softwares, IMAGELAB and IMAGETOOL, was used in the visualization. The image processor offers a real time grabbing technique so as to digitize an image quickly. An image-processing monitor can be used to show the images recorded by the CCD camera in real time, the images recorded in video tapes, and the enhanced images treated by the image processor. Thus, the better the image display is, the clearer the image is. The image display used in the present research was a high-resolution NEC MULTISYNC II color monitor. The color monitor can supply 256 colors or 256 black/white gray-levels. The 256 kinds of gray-levels are enough for us in dealing with images. In addition, two kinds of image outputs are displayed in the present study: one is the picture taken by a NIKON camera (Model: FM2), and the other is the figure plotted with a BENSON high-resolution color thermal plotter (Model: CTP-10), which is controlled by an APOLLO workstation (Model: DN-3000).

Experimental procedures

Prior to the operation of the transient experiments, all the measuring instruments were calibrated, and the test plates vertically and properly installed in the test section of the wind tunnel. In general, the experimental procedure included the following steps in an experimental sequence: experimental preparations, velocity measurement (first time), input heating-power measurement (first time), temperature measurement in the power-on transient period, temperature measurement in the steady-state period, input heating-power measurement (second time), smoke flow visualization with recording flow-fields, and velocity measurement (second time).

It should be noticed that the power-on transient period in the present experiments is the first 30 min after the power is switched on. The transient heat fluxes such as q_c'', q_k'', q_r'', and q_t'' varied sharply with time at the beginning of the period, and thus the time interval between data recordings was set at 1 min for the first 10 min, at 2 min for the successive 30 min and then at 5 min thereafter until the steady-state was reached. As we know, the performances of thermofoil heaters are affected because their temperatures vary with time during the experiments. For accurate measurement of output power generated by the d.c. power supplies, a double-check of the voltage output values was necessary during the experiments.

Data reduction

The objective of data reduction in the experiments is to use an effective model to calculate transient heat losses of the rib-heated test plate and to obtain an accurate transient convective heat flux, so as to get the transient local and average rib Nusselt numbers in the test channel.

Similar to the energy conservation concept for transient natural convection experiments presented by Hung and Shiau [19], it may be proposed that the total heat generated by thermofoil heaters for rib j, $Q_{i,j}$, is converted into the following four heat transfer modes at any specific transient time: (1) radiative heat loss, $Q_{r,j}$; (2) conductive heat loss, $Q_{k,j}$; (3) internal energy change of the test plate, $Q_{t,j}$; (4) convective heat dissipation in the test channel, $Q_{c,j}$. That is,

$$Q_{c,j} = Q_{i,j} - Q_{r,j} - Q_{k,j} - Q_{t,j}. \quad (1)$$

This energy-balance equation calculates the net transient convective heat flow rate, Q_c, from the test surface to the air in the test channel. The total power input to each rib is $Q_{i,j}$ and it equals V_j^2/R_j. Here, V_j represents the output voltage of each d.c. power supply and R_j the resistance of each thermofoil heater. $Q_{r,j}$ is the radiative heat loss from the stainless steel surface to its surroundings. It is evaluated with thermal diffuse gray-body networks. Based on the method of estimating the radiative heat losses in a channel with cubical elements by Ortega and Moffat [20], modified thermal radiation networks for a vertical ribbed channel, which establish the relationships of radiative interactions among rib surfaces, the base wall, the shrouding wall, and the ambient surroundings, were successfully developed in ref. [15]. According to the results of radiation analysis, the maximum radiative heat loss is less than 1.1% of the total input power for all the cases considered in the present study. $Q_{k,j}$ is the

conductive heat loss to the insulated PCB and balsa slab. It is evaluated by one-dimensional (for the PCB) and two-dimensional (for the balsa slab) conduction models [15]. In the present experiments, $Q_{k,j}$ varies from 8.0% to 11.3% for each rib of the typical case. $Q_{t,j}$ is the internal energy change of the stainless steel sheet and balsa wood during the experimental period. In the present analysis, an experimental method for estimating the internal energy change of the test plate during the power-on transient period was postulated. The expression of the internal energy change at a certain time during the transient period is

$$Q_{t,j} = Q_{s,j} + Q_{b,j}, \quad (2)$$

where $Q_{s,j} = (\rho C_p V \Delta \bar{T}/\Delta t)_{s,j}$ and $Q_{b,j} = (\rho C_p V \Delta \bar{T}/\Delta t)_{b,j}$. They represent the transient internal energy changes in the stainless steel sheet and the balsa wood for rib j, respectively; $\rho C_p V$ is the heat capacity of each material; $\bar{T}_{s,j}$ the average temperature of the SS304 sheet; $\bar{T}_{b,j}$ the average temperature of the balsa wood; and Δt the time interval. Consequently, the transient internal energy change of the test plate is estimated with reasonable accuracy.

Before the transient and steady-state results are displayed, it is necessary to clarify the power-on transient period and the steady-state condition of each experiment. Usually, the steady-state condition is considered to be achieved when all the $Q_{t,j}$ approach zero: $Q_{r,j}$ and $Q_{k,j}$ reach their steady-state values respectively; and all the $Q_{c,j}$ variations with time are less than 1.0% of the previous $Q_{c,j}$ values in each experiment. In general, the steady-state condition can be achieved about 30 min after the power is switched on. Furthermore, to ensure the reliability of the experimental steady-state results, a group of data with a minimum absolute $Q_{t,j}/Q_{i,j}$ value during the steady-state period were chosen as the data base for each case. Accordingly, the power-on transient period was defined as the time elapsed to achieve the steady-state condition after the power was switched on.

During the transient period, the values of $Q_{i,j}$, $Q_{r,j}$, $Q_{k,j}$ and $Q_{t,j}$ at any specified time t can be evaluated by equations (1) and (2); the net transient convective heat dissipation rate from the stainless steel surface of each rib, i.e. $Q_{c,j}$, can be obtained. Subsequently, the local and average rib Nusselt numbers in the power-on transient period are finally calculated.

Uncertainty analysis

Uncertainty and sensitivity analysis was used extensively in the experimental planning stage to help design the apparatus and data reduction procedures. The method used was the standard single-sample uncertainty analysis recommended by Kline and McClintock [21] and Moffat [22]. In the experiments, temperature measurements were accurate to within $\pm 0.2^{\circ}$C, the uncertainty of the heat flux q_j'' was determined to be 0.25%, and those of Re and Nu for the ranges of parameters studied in the power-on transient period were within 6.24% and 9.37%, respectively; in contrast to the steady state, that of Nu was within 4.54%.

EXPERIMENTAL RESULTS AND DISCUSSION

The present experimental results mainly emphasize the power-on transient forced convection heat transfer characteristics using a turbulence promoter in a vertical rib-heated channel. The test channel used in the experiments is shown in Fig. 1. The discrete heating ribs were made 2.0 cm long and 1.0 cm high (i.e. $B = 1.0$ cm) and the ratio of rib pitch height S/B was designed as 4.0. Five parameters of interest are the steady-state convective heat flux from the rib-heated test plate q_{cs}'', channel inlet velocity U_0, ratio of channel spacing to rib height H/B, promoter location LP, and ratio of promoter height to channel spacing t/H. The ranges of the above parameters studied in the transient experiments were $q_{cs,j}'' = 200$–630 W m^{-2}; $U_0 = 1.27$–5.76 m s^{-1}; $H/B = 2.5$–10; $t/H = 0.125$–0.6; and $LP = 1$, 2, 3, or 4, i.e. LP is chosen at one of the designed locations shown in Fig. 1. One hundred and seven data sets for cases with various above-mentioned parameter combinations are presented. In this study, the case with $H/B = 5.0$, $t/H = 0.2$, $LP = 3$, $U_0 = 3.84$ m s^{-1} and $q_{cs,j}'' = 358$ W m^{-2} for each of the four ribs was chosen as the typical one to interpret the primary heat transfer characteristics.

For conventional heat transfer study in forced convection, the channel inlet temperature T_0 is usually chosen as a reference to explore heat transfer phenomena in vertical channels, especially for the study of the channel-spacing effect on heat transfer characteristics. Therefore, the same reference is chosen in the present study.

The spanwise dimension of the test channel was 38.0 cm, an adequate width to assume a two-dimensional flow for the channel spacings studied in the experiments. This assumption can be verified from the measurement of spanwise temperature distributions. The spanwise temperatures on the test surface were measured along three columns. The span between two adjacent columns, measured in the direction normal to the streamwise air flow, was 10 cm. There were 46 calibrated T-type thermocouples installed along the streamwise direction in each column. As compared with local measured temperatures at the center column of the test section, the maximum deviations of the spanwise temperatures for the left column and the right column were less than 7.6% and 3.7%, respectively, in the range of parameters studied. This spanwise uniformity is consistent with the measured results for the 90° rib configuration without promoters at $Re = 12\,500$–$28\,500$ presented by Metzger *et al.* [23]. Therefore, the assumption of a two-dimensional distribution may be assured during the transient period, and the temperature distributions along the middle column were employed as representative of the whole test surface in the experiments.

Definition of rib heat transfer parameters

Similar to the steady-state definitions presented in ref. [17], the local and average transient heat transfer coefficients for each rib can be respectively expressed as

$$h_{x,j} = q''_{c,j}/(T_{wx,j} - T_0) \tag{3}$$

and

$$h_j = \frac{1}{L_r}\int_0^{L_r} h_{x,j}\,\mathrm{d}x, \tag{4}$$

where j represents the rib number and L_r the total heating length of each rib, i.e. $L_r = 2B + L$. During the power-on transient period, the net transient convective heat fluxes $q''_{c,j}$ for rib j in the channel increase with increasing measuring time. However, they are kept almost the same in the steady-state period, by means of controlling the four power supplies independently, for each experimental case. For instance, the steady-state heating conditions of the four ribs for the typical case are $q''_{es,1} = 357.32$ W m^{-2}, $q''_{es,2} = 358.23$ W m^{-2}, $q''_{es,3} = 358.07$ W m^{-2} and $q''_{es,4} = 356.38$ W m^{-2}, respectively.

Then, the average Nusselt number based on the rib height B ($B = 1$ cm in the present experiments) for rib j is

$$Nu_j = h_j B/k. \tag{5}$$

Consequently, the overall average Nusselt number, denoted by $\overline{Nu}$, in the channel can be evaluated as the average value of the Nusselt numbers of the four heating ribs.

From the experimental steady-state results reported in ref. [17], two important conclusions were drawn in the paper: (1) the fully-developed (or 'quasi-equilibrium') high temperature region started at the third rib in the ranges of parameters studied in the steady-state forced convection experiments; and (2) the greatest Nusselt number enhancement occurs at the rib immediately downstream of the promoter. From the present transient results, it is seen that these two conclusions can also be properly applied to transient cases, so the heat transfer parameters such as $q''_{c,j}$, h_j and Nu_j at rib 3 may be considered as fully-developed values in the present study. Consequently, from the viewpoint of heat transfer enhancement in the fully-developed region, the thermal characteristic at rib 3 is definitely the most interesting one to explore for cases with the installation of a turbulence promoter in the present transient study.

Transient convective heat flux distribution

According to the results of heat distributions for all the cases in the present experiments, it can be reasonably found that the internal energy change of the rib-heated test plate $Q_{t,j}$ decreases with increasing measuring time. The radiative heat loss $Q_{r,j}$, the conductive heat loss $Q_{k,j}$, and the heat convected into the air $Q_{c,j}$ increase with time elapsed in the transient experiment. Furthermore, the effects of the steady-state convective heat flux, channel inlet velocity, channel spacing, and turbulence-promoter location and height on the distribution of transient convective heat flux $q''_{c,j}$ are shown in Figs. 2(a) and (b). Figure 2(a) presents the distribution of transient convective heat flux of any rib for the cases of $U_0 = 3.84$ m s^{-1} and $H/B = 2.5$–10; $t/H = 0.0$–0.6; $q''_{es,j} = 200$–630 W m^{-2}; and $LP = 1$, 2, 3, or 4. In addition, Fig. 2(b) shows the $q''_{c,j}$ distribution of rib 3 for the cases of $H/B = 5$, $t/H = 0.2$, $q''_{es,j} = 358$ W m^{-2} and $LP = 3$ with the channel inlet velocity varied. In these figures, the transient convective heat flux $q''_{c,j}$ at any time is nondimensionalized by the convective heat flux in the steady-state for each rib, and the data profiles for all the ribs can be expressed in an exponential form as follows:

$$q''_{c,j}(t)/q''_{es,j} = 1.0 - \mathrm{e}^{-0.32t}, \tag{6}$$

where $q''_{c,j}(t)$ is the net heat flux convected to air at time t for rib j in the power-on transient period; $q''_{es,j}$ is the net heat flux convected to air for rib j in the steady-state; and t, expressed in minutes, is the time elapsed in the power-on transient period.

From Figs. 2(a) and (b), the results show that the effects of steady-state convective heat flux, channel spacing, and turbulence-promoter height and location on the $q''_{c,j}(t)/q''_{es,j}$ distribution ($j = 1$, 2, 3, or 4) are insignificant, as compared with the effect of channel inlet velocity.

Equation (6) can be used to evaluate the net heat flux convected to air for any rib j in the power-on transient period if the steady-state convective heat flux of the rib j is known. This formula is depicted as a generalized curve plotted in Figs. 2(a) and (b), and it fits very well for all the experimental data when the channel inlet velocity U_0 is greater than 2.00 m s^{-1}.

Furthermore, equation (6) is especially useful for the predictions of the time needed to achieve the steady-state condition. In general, we find from Figs. 2(a) and (b) that the steady-state condition will start approximately 30 min after the power is switched on when the channel inlet velocity U_0 is greater than 2.00 m s^{-1}. Besides, comparisons of equation (6) with other relevant experimental correlations proposed by Hung and Perng [24], Hung and Lee [25], Chang [15] and Chao [14] are also made here. In Hung and Perng's forced convection experiments, the test plate was a smooth vertical channel with isoflux heating; the proposed correlation in their power-on transient period was the same as equation (6). In Hung and Lee's forced convection experiments, a vertical channel with a two-dimensional rectangular rib under isoflux heating was explored. The experimental formula was presented in the following form:

$$q''_c(t)/q''_{es} = 1.0 - \mathrm{e}^{-0.25t}. \tag{7}$$

In Chang's natural convection experiments, the test channel was the same as the one used in the present

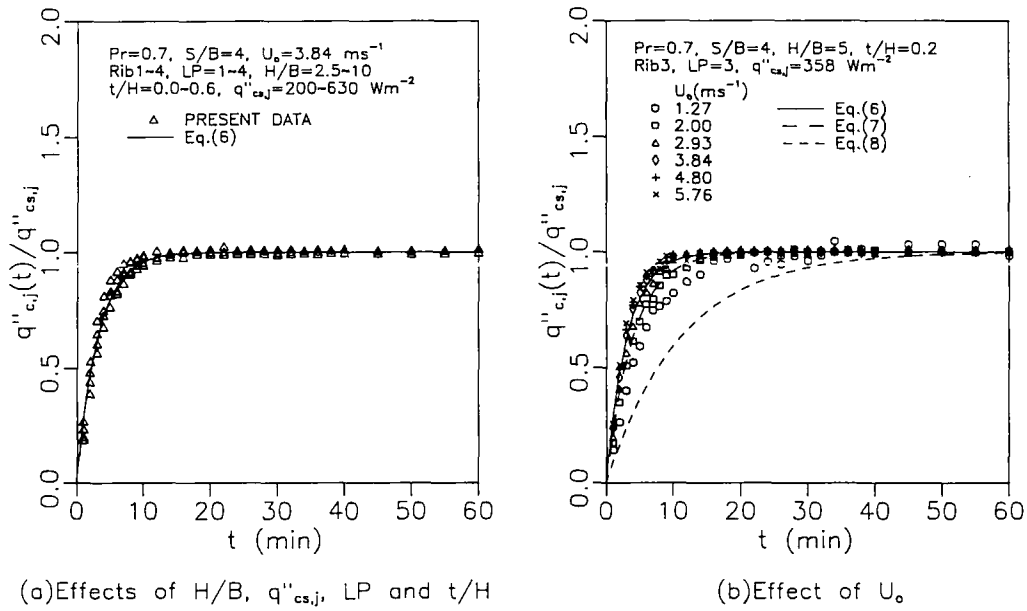

FIG. 2. Effects of relevant parameters on transient convective heat flux of ribs in the channel.

experiments but without a turbulence promoter. The experimental formula was proposed as

$$q''_c(t)/q''_{cs} = 1.0 - e^{-0.09t}. \quad (8)$$

In Chao's forced convection experiments, the test channel was also the same as the one used in the present experiments but without a turbulence promoter. The proposed correlation was also the same as equation (6). From the results, it is found that the installation of promoter has no significant effect on the $q''_{c,j}(t)/q''_{cs,j}$ distribution in the present experiments.

From the comparisons among the above-mentioned relevant correlations, it is interesting to point out that the tendency of achieving steady-state conditions in Chao's and the present studies is almost the same as Hung and Perng's forced convection results for a smooth asymmetric isoflux heating channel. The main reason may be that the ratio of rib pitch to rib height S/B is 4.0 in the studies, and a weak cavity flow occurs between any two adjacent ribs for $3 \leqslant S/B \leqslant 5$ [26]; accordingly, the heat transfer characteristics are similar to those for a smooth heating surface. In addition, for cases with channel inlet velocity U_0 smaller than 2.00 m s^{-1}, the experimental data deviate from equation (6). When the channel inlet velocity further decreases, the data will reasonably tend towards Chang's natural convection correlation, i.e. equation (8).

Transient heat transfer characteristics of ribs

Figure 3 shows the distributions of transient average Nusselt number of ribs for a typical case. From the results presented in the figure, it is interesting to find that Nu_j almost equals the steady-state value for each rib when $t \geqslant 3$ min in the transient period. This means that the rib Nusselt numbers in the transient period of $t \geqslant 3$ min are the same as that in the steady-state period. However, Nu_j deviates from the steady-state value for the duration of the first 3 min of the transient period. These results may be primarily caused by larger measuring uncertainties of experimental instruments in the first 3 min.

In Fig. 3, the results presented in Chao's experiments [14], which dealt with the same test channel as the one used in the present study but without a turbulence promoter, are plotted for comparison. It shows that the heat transfer characteristics of ribs 3 and 4 for cases without a promoter or the present typical case with a promoter have the same trend during both the power-on transient and steady-state periods, and the relative deviation of heat transfer characteristics between them can be neglected if the experimental uncertainty is taken into consideration. Consequently, it proves that the so-called 'fully-developed' (or 'quasi-equilibrium' high temperature) region starts at rib 3 in the parameter ranges studied in the present experiments. This conclusion is consistent with those reported by Arvizu and Moffat [2] for the study of a dense array of flat packs and by Faghri *et al.* [16] for the study of regular in-line arrays of rectangular blocks in forced air cooling.

In addition, it obviously indicates that the use of a turbulence promoter can effectively improve the heat transfer performance in the fully-developed region. Furthermore, it also reveals that during the power-on transient and steady-state periods, the use of a turbulence promoter not only increases the Nusselt numbers of its downstream ribs but also increases the Nusselt numbers of its upstream ribs.

As shown in Fig. 3, two other relevant results are

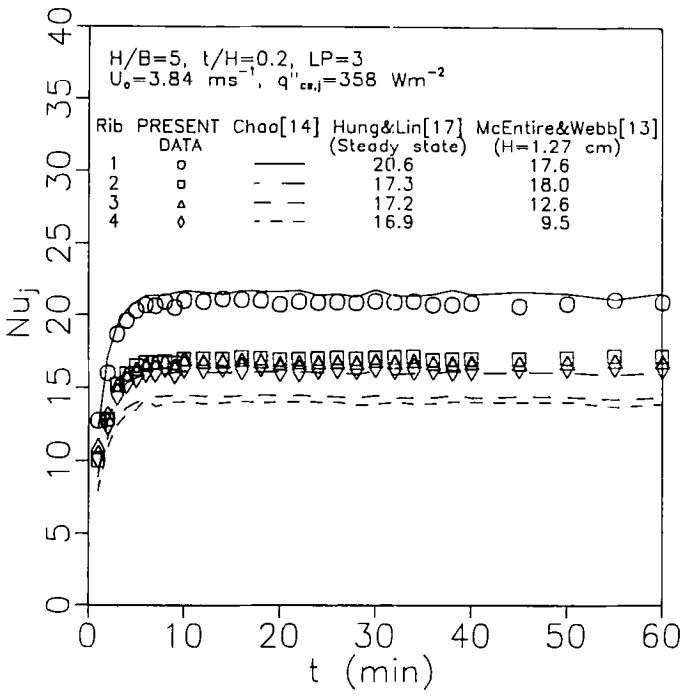

FIG. 3. Transient Nusselt numbers of ribs for a typical case.

also listed for comparison. The first one is the steady-state Nusselt numbers predicted by the following correlations, which were proposed by Hung and Lin [17]:

$$Nu_{s,j} = a\,Re^{0.55}(H/B)^{-0.75}[1 + b\,e^{-0.02(j-LP)^2}(t/H)], \tag{9}$$

with

$$j = \begin{cases} 1: a = 0.392, b = 0.0323 \\ 2: a = 0.303, b = 0.485 \\ 3: a = 0.263, b = 1.255 \\ 4: a = 0.252, b = 1.448 \end{cases}$$

and

$$\overline{Nu}_s = 0.302\,Re^{0.55}(H/B)^{-0.75}[1 + 0.692(t/H)], \tag{10}$$

where Nu_s is based on the rib height B and steady-state convective heat flux $q''_{cs,j}$. The maximum deviations of the predictions using the above correlations from the steady-state experimental data are 2.4% (rib 1), 2.6% (rib 2), 3.2% (rib 3) and 4.5% (rib 4), respectively.

The second one is calculated from the correlations of steady-state Nusselt numbers for flush-mounted heater configurations proposed by McEntire and Webb [13]:

$$Nu_{s,j} = \begin{cases} 0.772\,Re^{0.39}, & j = 1 \\ 0.574\,Re^{0.43}, & j = 2 \\ 0.372\,Re^{0.44}, & j = 3 \\ 0.576\,Re^{0.35}, & j = 4, \end{cases} \tag{11}$$

where the above correlations were valid for the cases of $H = 1.27$ cm and $L = 1.27$ cm for the range of $Re = 525$–3937. The comparisons of the present data with the predictions from McEntire and Webb's correlations display the significant effect of the installation of ribs and turbulence promoter for heat transfer augmentation in a vertical rib-heated channel.

Prior to investigating the effects of the steady-state convective heat flux $q''_{cs,j}$, channel inlet velocity U_0, ratio of channel spacing to rib height H/B, turbulence promoter location LP, and ratio of turbulence promoter height to channel spacing t/H on transient heat transfer characteristics in a rib-heated channel, several Nusselt numbers of interest such as Nu_{fd}, $\overline{Nu}$ and Nu_1 should be defined and chosen for interpreting heat transfer phenomena. Nu_{fd} is defined as the fully-developed Nusselt number, so it represents the heat transfer performance in the fully-developed region. In the present study, Nu_{fd} is set as the Nusselt number at rib 3 (i.e. Nu_3). $\overline{Nu}$ is the average heat transfer performance in the whole rib-heated channel. Besides, Nu_1 is the Nusselt number at rib 1 and represents the heat transfer performance of the first rib in the channel entrance region. From the present results, it is found that the average deviation of Nu_1 values for the corresponding cases with or without a turbulence promoter is 4.38%. This reveals that the installation of a promoter does not significantly affect Nu_1 in the ranges of parameters studied, so a ratio of Nu_{fd} to Nu_1, r_{fd}, is defined as the drop in the Nusselt number value from the entrance to the fully-developed region. It represents the heat transfer defect from the first rib of the entrance region to the rib of the fully-developed

region in the rib-heated channel. The effects of relevant parameters on transient heat transfer performance are discussed in the following.

Effect of steady-state convective heat flux. Figures 4(a)–(c) show the effect of the steady-state convective heat flux on Nu_{fd}, $\overline{Nu}$ and r_{fd}, respectively. From Figs. 4(a) and (b), it is found that the steady-state convective heat flux has no significant effect on transient Nusselt numbers in the present study. This shows that the heat transfer performance in the present experiments is not affected by buoyancy, and the heat transfer mechanism may be considered as purely forced convection. For comparison, the predicted steady-state Nu_{fd} and $\overline{Nu}$ from the correlations presented in ref. [17] with various $q''_{cs,j}$ values, i.e. equations (9) and (10), are listed in Figs. 4(a) and (b), respectively. The maximum deviations of the predicted Nu_{fd} from the steady-state experimental data are 6.9, 5.2, 3.2, 1.4, 4.7 and 2.4% for $q''_{cs,j} = 200$, 280, 358, 450, 540 and 630 W m^{-2}, respectively; the corresponding deviations for $\overline{Nu}$ are 4.5, 3.2, 2.0, 2.8, 10.2 and 1.9%.

Furthermore, the r_{fd} distributions in the power-on transient period for the present cases with a promoter under various steady-state convective heat fluxes are presented in Fig. 4(c); those for the cases without a promoter [14] are also shown in the figure for comparison. In Fig. 4(c), the r_{fd} values are not affected by the steady-state convective heat flux and are kept almost constant in the transient and steady-state periods. The r_{fd} value is 0.78 for the cases with a turbulence promoter located at $LP = 3$, and 0.66 for the cases without a turbulence promoter. Therefore, it also confirms the conclusion made in Fig. 3; that is, the use of a turbulence promoter can effectively improve the heat transfer performance in the fully-developed region.

Effect of channel inlet velocity. As for the effects of channel inlet velocity, the results are shown in Fig. 5(a)–(c), respectively, for Nu_{fd}, $\overline{Nu}$, and r_{fd}. For the cases of $H/B = 5$, $t/H = 0.2$, $LP = 3$ and $q''_{cs,j} = 358$ W m^{-2} with various inlet velocities, it is found that the transient Nusselt number increases with increasing channel inlet velocity (Figs. 5(a) and (b). This observation agrees with what is physically expected in forced convection. The predicted steady-state Nu_{fd} and $\overline{Nu}$ from the correlations presented in ref. [17] with various U_0 values, i.e. equations (9) and (10), are listed in Figs. 5(a) and (b), respectively. The maximum deviations of the predicted Nu_{fd} from the steady-state experimental data are 10.9, 4.7, 6.9, 3.2, 6.2 and 6.4% for $U_0 = 1.27$, 2.00, 2.93, 3.84, 4.80 and 5.76 m s^{-1}, respectively; those for $\overline{Nu}$ are 14.2, 4.1, 5.8, 2.0, 4.3 and 4.6%. In these figures, the natural convection results reported in ref. [15], where the test channel is the same as the one used in the present experiments but without turbulence promoter, are also shown for reference. The trend of the present experimental data will reasonably approach the natural convection result when the channel inlet velocity decreases.

The r_{fd} distributions in the power-on transient period for the cases with a turbulence promoter under different channel inlet velocities are presented in Fig. 5(c); those for the cases without a turbulence promoter [14] are also shown for comparison. In this figure, r_{fd} decreases with increasing channel inlet velocity for the cases with or without a promoter. This tendency is consistent with the results observed by Faghri *et al.* [16]. They concluded that the Nusselt number in the entrance region was high and was a strong function of velocity; also, the Nusselt number was strongly dependent on row number for higher channel inlet velocity, whereas the Nusselt number profile looked quite flat for lower channel inlet velocity.

Similar to the results presented in Fig. 4(c), the r_{fd} values for the cases under a specified channel inlet velocity, as shown in Fig. 5(c), were kept almost constant during the transient and steady-state periods. r_{fd} varied between 0.77 and 0.85 for the cases with a promoter located at $LP = 3$, while the ratio ranged from 0.61 to 0.72 for the cases without a promoter. Therefore, this observation also indicates that the use of a turbulence promoter can effectively enhance the heat transfer performance in the fully-developed region.

Effect of channel spacing. For investigating the effect of channel spacing on transient heat transfer characteristics, Figs. 6(a)–(c) show the results for the cases of $t/B = 1.0$, $LP = 3$, $U_0 = 3.84$ m s^{-1} and $q''_{cs,j} = 358$ W m^{-2} with various channel spacings. In Figs. 6(a) and (b), it is seen that the transient Nusselt numbers Nu_{fd} and $\overline{Nu}$ increase when the H/B ratio decreases. This tendency can reasonably be explained by the magnitude of flow acceleration occurring in the effective contraction passage of the channel for various H/B ratios. As we know, when the channel inlet velocity is fixed, say $U_0 = 3.84$ m s^{-1}, the cross-sectional area of the free flow passage formed by the obstructive ribs and the turbulence promoter decreases with decreasing channel spacing; the effective flow velocity will increase and the heat transfer performance will consequently be improved if the channel spacing decreases. Thus, it may be concluded that the smaller the channel spacing the larger the transient Nusselt number for each rib. This is consistent with the results reported in ref. [16] for both the fully-developed and entrance regions. Furthermore, the steady-state Nu_{fd} and $\overline{Nu}$ predicted from the correlations presented in ref. [17] with various H/B values, i.e. equations (9) and (10), are listed in Figs. 6(a) and (b), respectively. The maximum deviations of the predicted Nu_{fd} from the steady-state experimental data are 16.9, 8.4, 10.0, 3.2, 2.3 and 7.2% for $H/B = 2.5$, 3.0, 4.0, 5.0, 6.0 and 8.0, respectively; those for $\overline{Nu}$ are 16.4, 6.8, 8.4, 2.0, 4.9 and 10.1%.

Moreover, the r_{fd} distributions in the power-on transient period for the cases with a turbulence promoter under different channel spacings are displayed in Fig. 6(c); those for the cases without a turbulence

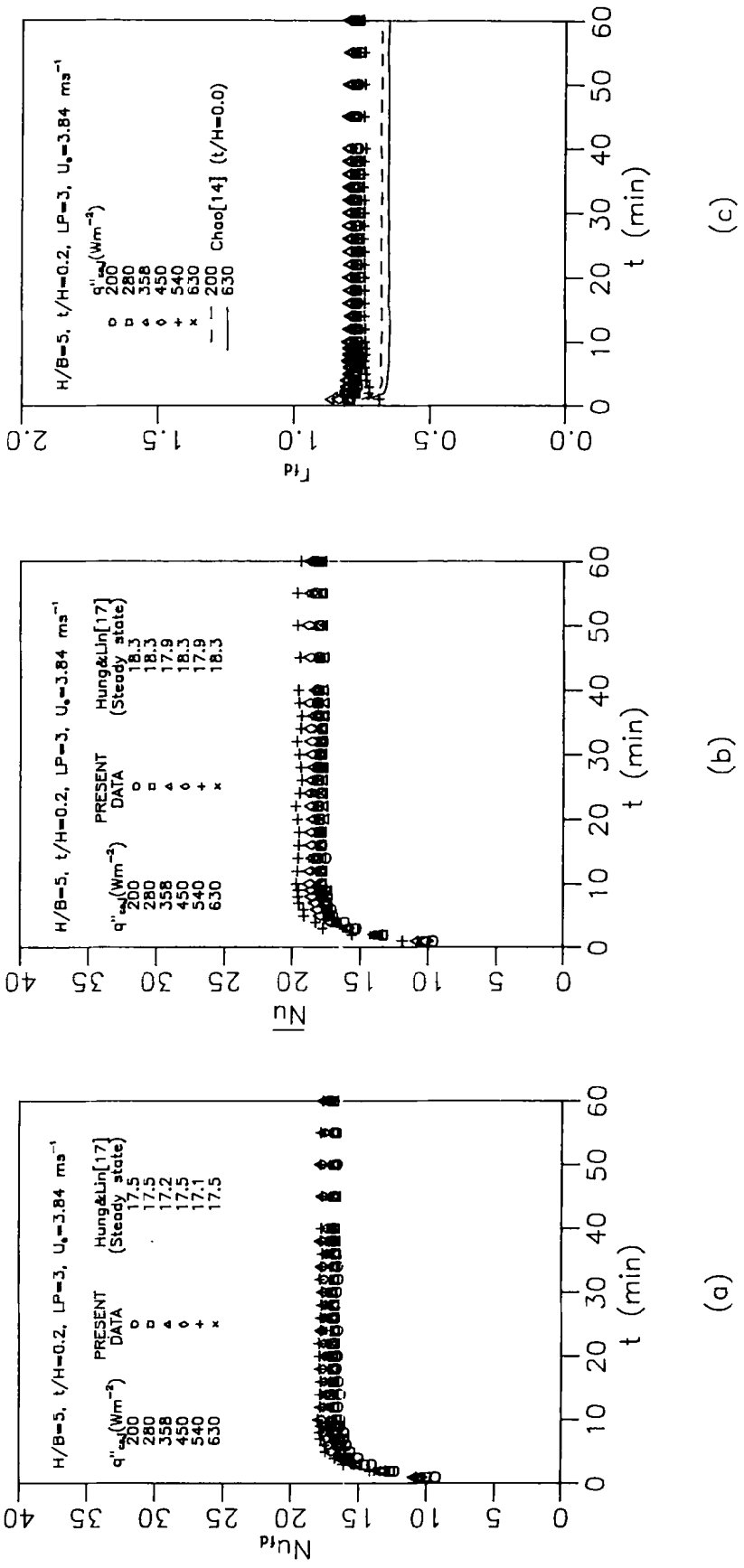

FIG. 4. Effect of q''_{conv} on transient Nusselt numbers and r_{fd} distributions: (a) Nu_{fd}; (b) $\overline{Nu}$; (c) r_{fd}.

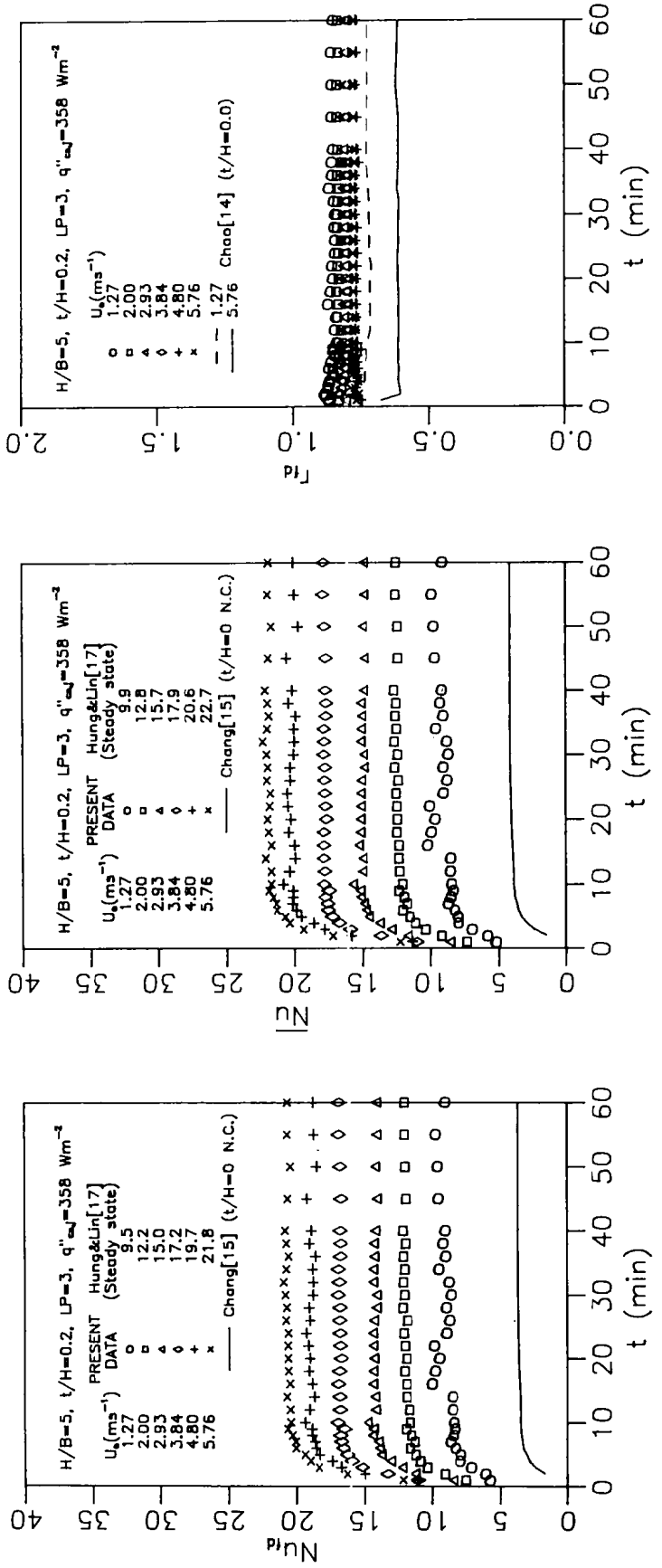

FIG. 5. Effect of U_0 on transient Nusselt numbers and r_{id} distributions: (a) Nu_{id}; (b) $\overline{Nu}$; (c) r_{id}.

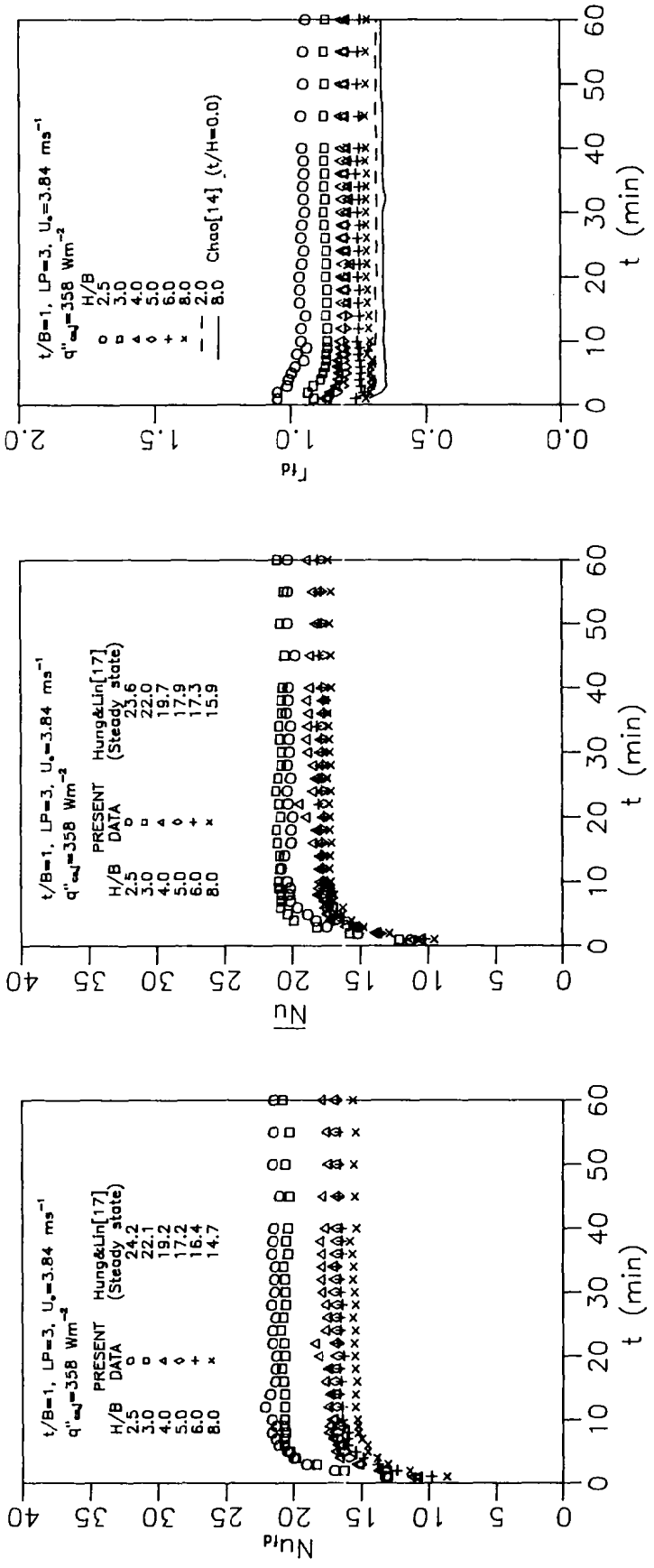

FIG. 6. Effect of H/B on transient Nusselt numbers and r_{rd} distributions: (a) Nu_{rd}; (b) $\overline{Nu}$; (c) r_{rd}.

promoter [14] are also shown for comparison. In this figure, it is evident that r_{fd} increases with decreasing channel spacing for the cases with a promoter, while the ratio is a weak function of channel spacing, i.e. the ratio is not significantly affected by channel spacing, for the cases without a promoter. This trend also indicates that the use of a turbulence promoter can effectively improve the heat transfer performance in the fully-developed region; the smaller the channel spacing, the stronger the effect of turbulence promoter. In addition, the r_{fd} values are kept almost constant during the transient and steady-state periods. For the cases with a promoter located at $LP = 3$, the r_{fd} ratios are 0.95, 0.87, 0.80, 0.80, 0.75 and 0.72 for $H/B = 2.5$, 3.0, 4.0, 5.0, 6.0 and 8.0, respectively; those for the cases without a promoter are 0.66–0.68.

Effect of turbulence promoter location. Figures 7(a)–(c) show the effect of turbulence promoter location on transient heat transfer characteristics. The results for the corresponding case without a turbulence promoter, presented in ref. [14], are also shown for comparison. From the transient results presented in Fig. 7(a), the same conclusion drawn for steady-state cases [17] can be applied to transient cases; that is, the greatest transient Nusselt number enhancement occurs at the rib immediately downstream of the promoter. With increasing upstream or downstream distance of the heating rib measured from the promoter, the extent of the heat enhancement gradually drops off. Nevertheless, as shown in Fig. 7(b), the effect of promoter location is insignificant on transient $\overline{Nu}$ distributions. Moreover, the steady-state Nu_{fd} and $\overline{Nu}$ predicted from the correlations presented in ref. [17] with different LP values, i.e. equations (9) and (10), are listed in Figs. 7(a) and (b). The maximum deviations of the predicted Nu_{fd} from the steady-state experimental data with various LP values are 14.2, 5.6, 3.2, 6.5 and 5.9% for the cases with $LP = 1$, 2, 3, 4 and the case without a promoter, respectively; those for $\overline{Nu}$ are 7.6, 1.6, 2.0, 2.2 and 5.5%.

The above experimental heat transfer characteristics can also be verified qualitatively by the observation of flow-fields through smoke flow visualization. From the smoke flow-fields treated by an image processing system, the effect of promoter location on flow-field for cases of $H/B = 5$, $t/H = 0.2$ and $U_0 = 1.00$ m s^{-1} is shown in Fig. 8. It is found that the maximum fluid velocity occurs at the cross-sectional plane of the effective contraction passage, formed by the promoter and the opposite rib immediately downstream of the promoter. The forced flow abruptly lifts off due to the presence of the promoter mounted on the shrouding wall, and transversely accelerates its velocity near the rib immediately downstream of the promoter. Thus, the heat transfer characteristics on the rib immediately downstream of the promoter will have the greatest heat transfer enhancement.

The r_{fd} distributions in the power-on transient period for the cases of $H/B = 5$, $t/H = 0.2$. $U_0 = 3.84$ m s^{-1} and $q''_{cs,j} = 358$ W m^{-2} with different LP values are presented in Fig. 7(c). From the figure, it is seen that the r_{fd} ratios are almost constant in the transient and steady-state periods, and weakly affected by promoter location except in the case with $LP = 1$. As compared with the results, shown in Figs. 7(a) and (c), for the case without a promoter, it may be concluded that the use of a turbulence promoter located at $LP = 1$ cannot improve the heat transfer performance for the ribs in the fully-developed region effectively.

Effect of turbulence promoter height. The effect of turbulence promoter height on transient heat transfer characteristics is shown in Figs. 9(a)–(c). These figures show that there is a significant effect of t/H ratio on transient Nu_{fd} and $\overline{Nu}$ distributions for the cases with $LP = 3$; the Nu_{fd} and $\overline{Nu}$ values increase with increasing t/H ratio. However, the effect of t/H ratio on transient Nu_1 at the first rib in the entrance region for the cases with a promoter installed at the location in the fully-developed region (i.e. $LP = 3$) is insignificant in the present experiments. These results verify that the use of a turbulence promoter in the fully-developed region can directly and effectively improve the heat transfer characteristics of this region, but its effect on the upstream rib in the entrance region is less significant. The steady-state Nu_{fd} and $\overline{Nu}$ evaluated from the correlations presented in ref. [17] for the cases with various t/H values, i.e. equations (9) and (10), are also listed in Figs. 9(a) and (b), respectively. Maximum deviations of the predicted Nu_{fd} from the steady-state experimental data for the cases with various t/H ratios ($t/H = 0$, 0.125, 0.167, 0.188, 0.200, 0.250, 0.375 and 0.563) are 5.9, 7.2, 2.3, 3.8, 3.2, 10.0, 8.4 and 7.3%, respectively; the corresponding deviations for $\overline{Nu}$ are 5.5, 10.1, 4.9, 6.9, 2.0, 8.4, 10.3 and 12.0%.

Moreover, the distributions of r_{fd} in the power-on transient period for the cases with various t/H values are presented in Fig. 9(c). The r_{fd} ratio increases with increasing t/H ratio for the cases with $LP = 3$ during the transient and steady-state periods. For the cases with $LP = 3$, the r_{fd} values are 0.67, 0.72, 0.75, 0.77, 0.80, 0.80, 0.96 and 1.07 for $t/H = 0$, 0.125, 0.167, 0.188, 0.200, 0.250, 0.375 and 0.563, respectively. This trend also indicates that the use of a turbulence promoter can enhance the heat transfer performance in the fully-developed region effectively.

Qualitatively, the effect of turbulence promoter height on heat transfer characteristics can also be interpreted through smoke fluid visualization. Figure 10 displays flow-fields, which are treated by the image processing system, for cases with $H/B = 5$, $LP = 3$ and $U_0 = 1.0$ m s^{-1}, to investigate the effect of promoter height on fluid field. From the figure, it is obviously found that the flow separates in the region immediately upstream from the first rib, and a boundary layer develops on the surface of rib 1. Then, the flow passes through an effective contraction passage formed by the obstructive ribs and the turbulence

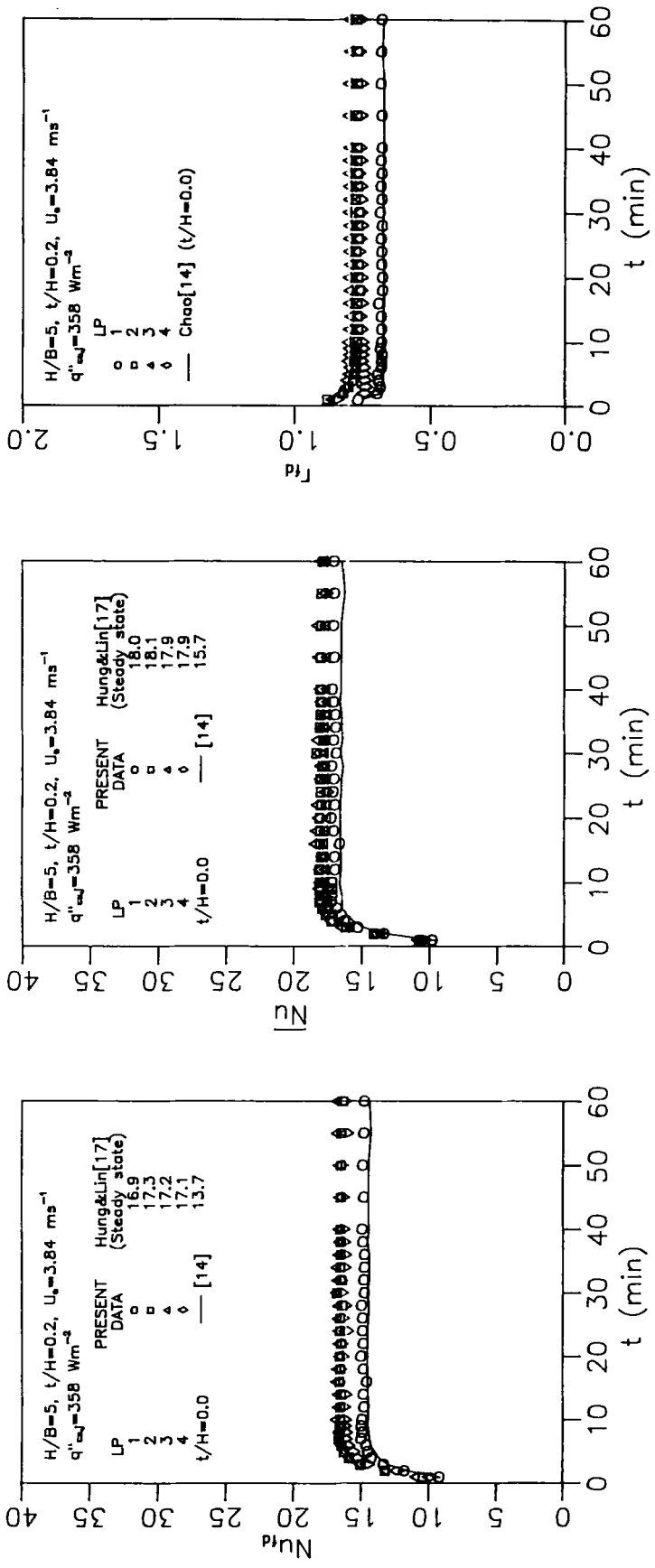

FIG. 7. Effect of LP on transient Nusselt numbers and r_{fd} distributions: (a) Nu_{fd}; (b) $\overline{Nu}$; (c) r_{fd}.

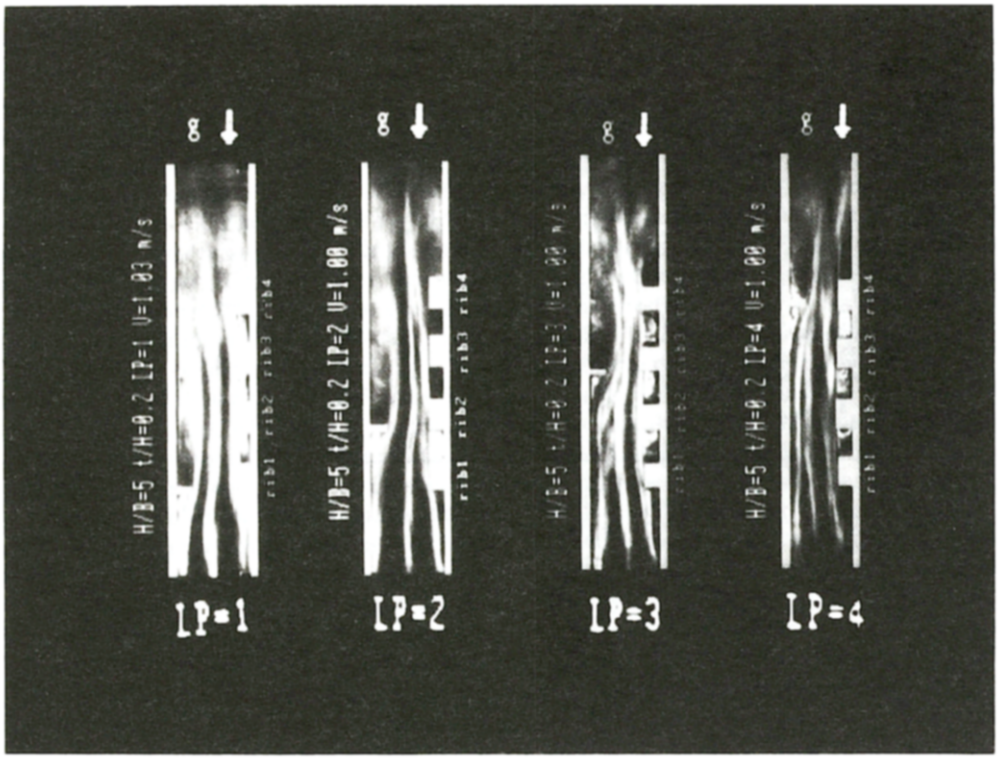

FIG. 8. Effect on LP on flow-field in the rib-heated channel.

promoter mounted on the opposite shrouding wall surfaces. Three weak recirculations occur in the cavities between two successive ribs; two recirculations generated in the upstream and downstream region of the promoter, respectively. When fluid flows through rib 4, a recirculation is found in the region immediately downstream of rib 4 due to the backward-step expansion. It is observed that the fluid is abruptly accelerated in the effective contraction passage of the channel due to the effects of rib obstructions and the promoter; consequently, as compared with the heat transfer performance for a ribbed channel without a turbulence promoter discussed in ref. [14], the heat transfer performance for the present ribbed channel is enhanced, especially in the opposite region of the promoter, i.e. the region near rib 3. The main reason is that the forced flow abruptly lifts off due to the presence of the promoter mounted on the shrouding wall, and transversely accelerates its velocity near the rib immediately downstream of the promoter. This inference from flow visualization is confirmed by the quantitative measurement results of heat transfer presented by Hung and Lin [17] and the present study.

In addition, from the observation of flow-fields, it is obvious that when the t/H ratio increases, the acceleration of fluid is increased in the effective contraction passage. It is interesting to notice that, when $t/H \leqslant 0.5$, the fluid is accelerated in the effective contraction passage and there is a recirculation generated in the region immediately behind the promoter, while a jet-like flow behavior can be found in the contraction passage and the flow directly impinges toward the downstream ribs. Furthermore, no circulation exists in the region immediately behind the promoter when $t/H \geqslant 0.563$. According to this flow pattern, the heat transfer performance of the rib immediately downstream of the promoter should be greatly improved when $t/H \geqslant 0.563$. However, a strong recirculation is observed in the region immediately ahead of the promoter when $t/H \geqslant 0.563$. This will cause a very large pressure loss in the channel. All the above is consistent with the conclusion mentioned above, i.e. a higher promoter provides more advantages for heat transfer enhancement; however, there is a severe penalty in pressure drop [17].

CONCLUDING REMARKS

An experimental investigation of transient forced convection heat transfer in a vertical rib-heated channel with a turbulence promoter has been systematically performed in the present study. The main conclusions emerging from this study may be drawn as follows.

(1) A generalized correlation for transient convective heat flux has been proposed in the present study and it fits very well for the experimental data when $U_0 \geqslant 2.0\ \mathrm{m\ s^{-1}}$. When the channel inlet velocity decreases further, the experimental data will reasonably tend toward the natural convection correlation.

(2) The effects of channel inlet velocity, compared

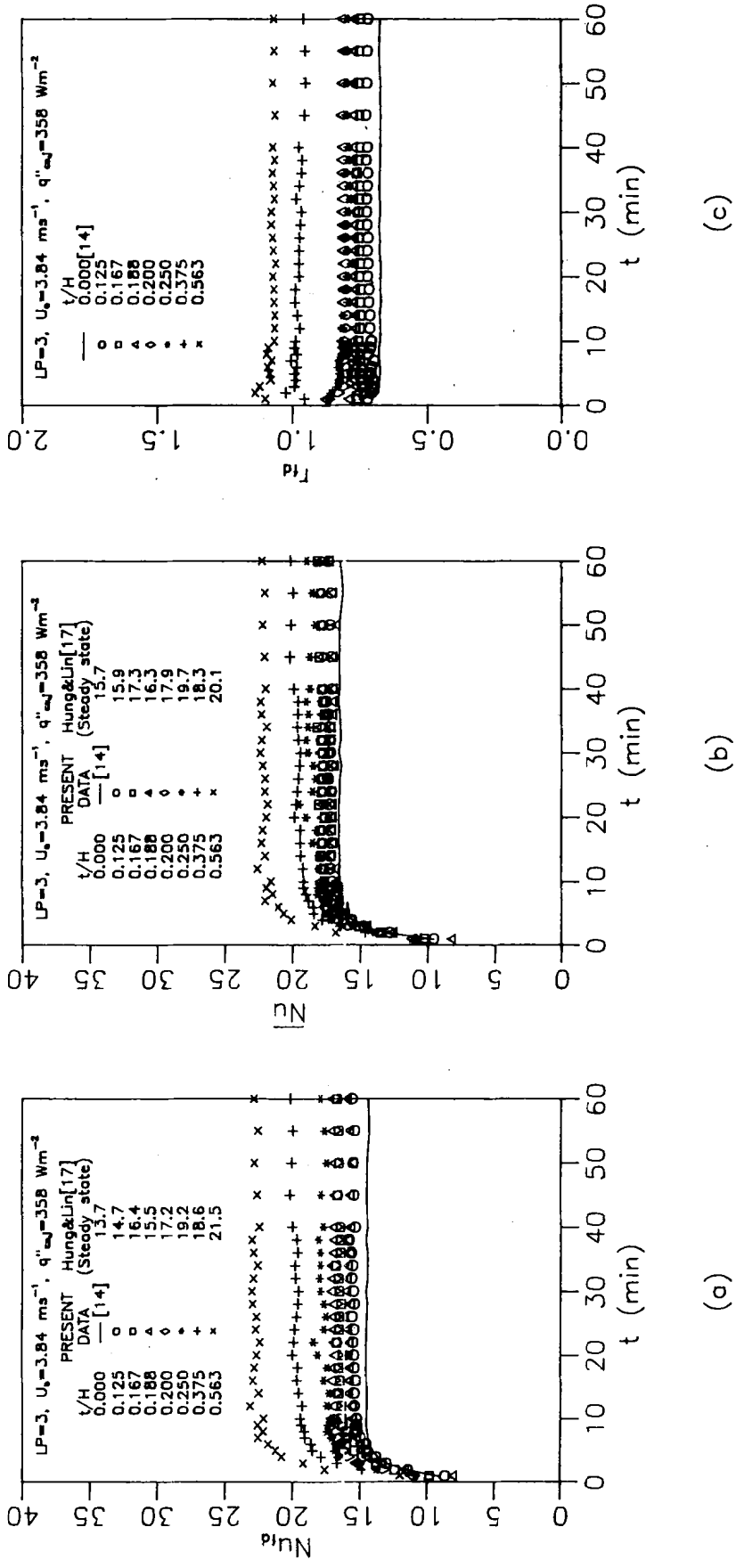

FIG. 9. Effect of t/H on transient Nusselt numbers and r_{rd} distributions: (a) Nu_{rd}; (b) $\overline{Nu}$; (c) r_{rd}.

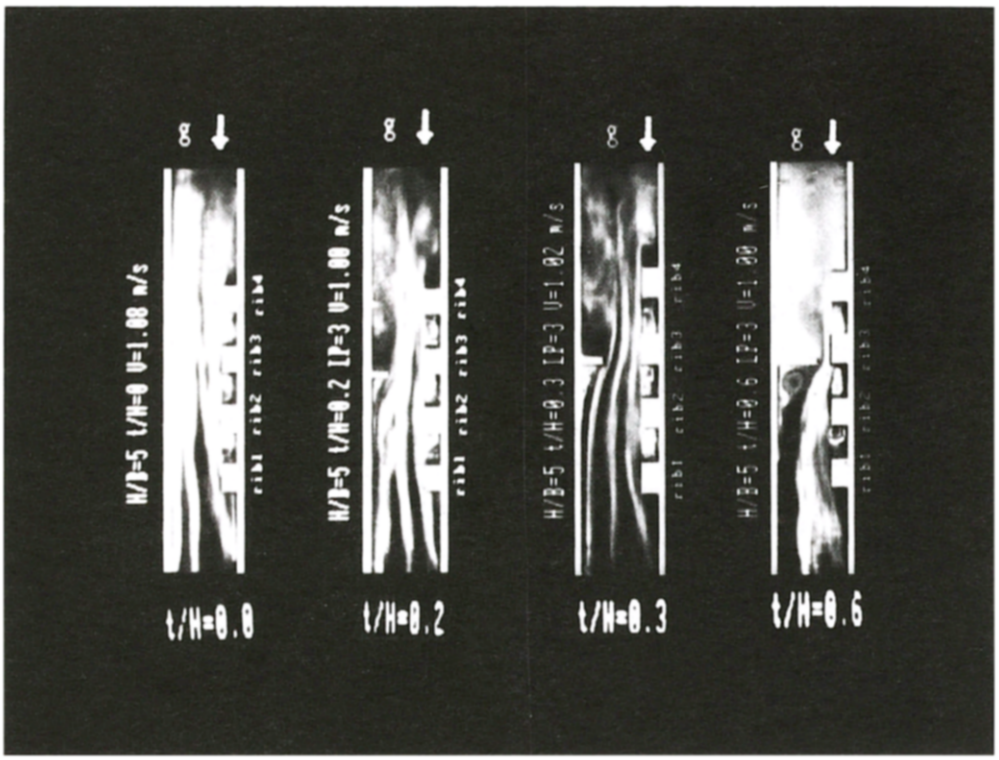

FIG. 10. Effect of t/H on flow-field in the rib-heated channel.

with other relevant parameters such as the steady-state convective heat flux, channel spacing, and turbulence promoter height and location, on $q''_{c,i}(t)/q''_{cs,i}$ and Nusselt number distributions are more significant in the experiments.

(3) Nu_i is close to the steady-state value except in the first 3 min of the power-on transient period. If the uncertainties in Nu_i are taken into consideration, the transient Nusselt numbers may be considered as the steady-state values during the power-on transient period.

(4) The use of a turbulence promoter can effectively improve the heat transfer performance in the fully-developed region. In addition, during the power-on transient period, it enhances not only the heat transfer performance of its downstream ribs, but also that of its upstream ribs.

(5) The transient heat transfer performance will increase when the H/B ratio decreases. In addition, τ_{fd} increases with decreasing channel spacing for cases with a promoter, while it is almost constant for cases without a promoter. This trend indicates that the smaller the channel spacing, the stronger the effect of turbulence promoter.

(6) The t/H effect is more significant than the promoter location on transient heat transfer performance, which increases with increasing t/H ratio. Besides, the use of a turbulence promoter located in the entrance region cannot effectively improve the heat transfer performance in the fully-developed region.

Acknowledgements—The authors gratefully acknowledge the support of the National Science Council, Taiwan, R. O. C. (under grant number NSC-78-0401-E-007-10). They also wish to thank Z. H. Lin for his assistance with the image-processing treatment of flow visualization results.

REFERENCES

1. L. A. Nelson, K. S. Sekhon and J. E. Fritz, Direct heat pipe cooling of a semiconductor devices, *Proc. Int. Heat Pipe Conf.*, pp. 373–376 (1978).
2. D. E. Arvizu and R. J. Moffat, Experimental heat transfer from an array of heated cubical elements on an adiabatic channel wall, Report No. HMT-33, Thermosciences Div., Dept. of Mech. Engng, Stanford University (1981).
3. E. M. Sparrow, J. E. Niethammer and A. Chaboki, Heat transfer and pressure drop characteristics of arrays of rectangular modules encountered in electronic equipment, *Int. J. Heat Mass Transfer* **25,** 961–973 (1982).
4. E. M. Sparrow, S. B. Vemuri and D. S. Kadle, Enhanced and local heat transfer, pressure drop, and flow visualization for arrays of block-like electronic components, *Int. J. Heat Mass Transfer* **26,** 689–699 (1983).
5. E. M. Sparrow, A. A. Yanezmoreno and D. R. Otis, Jr., Convective heat transfer response to height differences in an array of block-like electronic components, *Int. J. Heat Mass Transfer* **27,** 469–473 (1984).
6. J. Davalath and Y. Bayazitoglu, Forced convection cooling across rectangular blocks, *ASME J. Heat Transfer* **109,** 321–328 (1987).
7. Y. Asako and M. Faghri, Three-dimensional heat transfer and fluid flow analysis of arrays of square blocks encountered in electronic equipment, *Numer. Heat Transfer* **13,** 481–498 (1988).
8. Y. Asako and M. Faghri, Three-dimensional heat trans-

fer analysis of arrays of heated square blocks, *Int. J. Heat Mass Transfer* **32**, 395–405 (1989).
9. R. W. Knight and M. E. Crawford, Simulation of convective heat transfer in pipes and channels with periodically varying cross-sectional area. In *Numerical Methods in Thermal Problems* (Edited by R. W. Lewis and K. Morgan), Vol. 5, pp. 512–523. Pineridge Press, Swansea (1987).
10. R. W. Knight and M. E. Crawford, Numerical prediction of turbulent flow and heat transfer in channels with periodically varying cross section area. *Proc. 1988 National Heat Transfer Conf.*, Vol. 1, pp. 669–676. ASME, New York (1988).
11. G. L. Lehmann and R. A. Wirtz, The effect of variations in stream-wise spacing and length on convection from surface mounted rectangular components. In *Heat Transfer in Electronic Equipment–1985* (Edited by A. Ortega, D. Agonafer and B. W. Webb), ASME HTD Vol. 48, pp. 39–47. ASME, New York (1985).
12. K. Tarikoshi, M. Kawazoe and T. Kurihara, Convective heat transfer characteristics of arrays of rectangular blocks affixed to one wall of a channel. In *Natural and Mixed Convection in Electronic Equipment Cooling* (Edited by R. A. Wirtz), ASME HTD Vol. 100, pp. 59–65 (1988).
13. A. B. McEntire and B. W. Webb, Local forced convective heat transfer from protruding and flush-mounted two-dimensional discrete heat sources, *Int. J. Heat Mass Transfer* **33**, 1521–1533 (1990).
14. S. D. Chao, An experimental study on forced convection heat transfer characteristics in vertical adiabatic channels with surface-mounted heating ribs, Master's Thesis, Department of Power Mechanical Engineering, National Tsing Hua University, Taiwan, R.O.C. (June 1990).
15. N. T. Chang, An experimental study on heat transfer characteristics of natural convection in vertical channels with surface-mounted ribs, Master's Thesis, Department of Power Mechanical Engineering, National Tsing Hua University, Taiwan, R.O.C. (June 1989).
16. M. Faghri, A. Ray, S. Sridhar and R. Schmidt, Entrance heat transfer correlation for air cooling of arrays of rectangular blocks. In *Heat Transfer Enhancement in Electronics Cooling* (Edited by S. H. Bhavnani and M. Greiner), ASME HTD Vol. 183, pp. 19–23 (1991).
17. Y. H. Hung and H. H. Lin, An effective installation of turbulence promoters for heat transfer augmentation in a vertical rib-heated channel, *Int. J. Heat Mass Transfer* **35**, 29–42 (1992).
18. Y. H. Hung and W. M. Shiau, Local steady-state natural convection heat transfer in vertical parallel plates with a two-dimensional rectangular rib, *Int. J. Heat Mass Transfer* **31**, 1279–1288 (1988).
19. Y. H. Hung and W. M. Shiau, An effective model for measuring transient natural convection heat flux in vertical parallel plates with a rectangular rib, *Int. J. Heat Mass Transfer* **32**, 863–871 (1989).
20. A. Ortega and R. J. Moffat, Experimental on buoyancy-induced convection heat transfer from an array of cubical elements on a vertical channel wall, Report No. HMT-38, Thermosciences Div., Dept. of Mech. Engng, Stanford University (1986).
21. S. J. Kline and F. A. McClintock, Describing uncertainties in single-sample experiments, *Mech. Engng* 3–8 (Jan. 1953).
22. R. J. Moffat, Describing the uncertainties in experimental results, *Exp. Therm. Fluid Sci.* **1**, 3–17 (1988).
23. D. E. Metzger, C. S. Fan and Y. Yu, Effects of rib angle and orientation on local heat transfer in square channels with angled roughness ribs. In *Compact Heat Exchangers* (Edited by R. K. Shah, A. D. Kraus and D. E. Metzger), pp. 156–158. Hemisphere, New York (1990).
24. Y. H. Hung and S. W. Perng, An experimental technique for measuring transient natural/forced-convective heat fluxes in a vertical channel, *Exp. Therm. Fluid Sci.* **1**, 305–313 (1988).
25. Y. H. Hung and D. Y. Lee, Transient forced-convective heat transfer in a vertical channel mounted with a rectangular rib. In *Transfer Phenomena in Thermal Control* (Edited by G. J. Hwang), pp. 115–126. Hemisphere, New York (1989).
26. C. K. Liu, S. J. Kline and J. P. Johnston, An experimental study of turbulent boundary layers on rough walls, Ph.D. Thesis, MD-15, Department of Mechanical Engineering, Stanford University, U.S.A. (1966).